ELSEVIER

Biomaterials 24 (2003) 769–775

Biomaterials

www.elsevier.com/locate/biomaterials

Characterization of the bone-like apatite precipitated on high velocity oxy-fuel (HVOF) sprayed calcium phosphate deposits

K.A. Khor[a,*], H. Li[a], P. Cheang[b]

[a] School of Mechanical and Production Engineering, Nanyang Technological University, 50 Nanyang Avenue, Singapore 639 798, Singapore
[b] School of Materials Engineering, Nanyang Technological University, 50 Nanyang Avenue, Singapore 639798, Singapore

Received 19 February 2002; accepted 29 August 2002

Abstract

Bone-like apatite was precipitated on the surface of thermal sprayed calcium phosphate coatings following in vitro incubation in a simulated body fluid. The coatings were initially deposited on titanium alloy substrates by the high velocity oxy-fuel (HVOF) spray technique. Structural characterization and mechanical evaluation of the precipitated apatite layer were conducted. Results showed that the precipitation rate was directly influenced by the local Ca^{2+} concentration in the vicinity of the coating's surface and that preferential dissolution of certain phases was found to accelerate the precipitation of the bone-like apatite. The dense precipitates exhibited a competitive Young's modulus value of $\sim$120 GPa, which was obtained through nanoindentation. This compared favorably to the calcium phosphate matrix. Differences in microstructure at various locations within the layer resulted in altered Young's modulus and microhardness values. Precipitation mechanism investigation was carried out through a comparative experiment. Chemical analysis showed that the precipitation of bone-like apatite on the calcium phosphate coating was quite conceivably a partial diffusion-controlled process.

Keywords: Calcium phosphate; Coating; In vitro; SBF; Precipitates; Bone-like apatite; HVOF; Nanoindentation

1. Introduction

Hydroxyapatite (HA) coatings deposited on titanium implants have shown promising effects on the rapid bone remodeling and, hence, suitable functional life in orthopedic and dental applications [1,2]. The tissue attachment was directly related to the type of tissue response at the bone/implant interface [3]. To date, it is apparent that the simplest form of interaction between implant materials and the biological environment is the transfer of chemical species (ions, atoms and molecules) across the material–tissue interface in the absence of any adverse reaction [3]. Therefore, the surface behavior of the coating/substrate implant is fundamental, contributing cogently to the overall implant fixation. Even though the biological environment of the implants experienced in vitro is remarkably different from that of in vivo, nevertheless in vitro tests have come to be recognized as precursors for more involved, more costly and time-consuming animal implantation. To date, numerous studies have approximately clarified the in vitro behavior of the calcium phosphate coatings deposited by thermal spray techniques [4–6]. It was claimed that different calcium phosphate phases exhibited different identified structures, and could thus lead to different biological responses in the simulated body fluid (SBF) [5]. It was believed that the intimate contact with the SBF initiated conspicuous changes in the HA coatings [7].

Generally, the in vitro behavior of calcium phosphate coatings primarily involves the dissolution/precipitation process. Variation of crystal structure and stoichiometry of the calcium phosphate ceramics produces mixed dissolution behavior. The dissolution rate of monophasic calcium phosphate ceramics increases in the following order: HA < CDHA < OHA < β-TCP < α-TCP < TTCP [5]. Furthermore, the influence of crystallinity of HA coatings has been clarified through in vitro test by immersing HA coating with varying amorphous phase (ACP) contents into SBF [5,6]. Ducheyne et al. [5]

*Corresponding author. Tel.: +65-6-790-5526; fax: +65-6-791-1859.
E-mail address: mkakhor@ntu.edu.sg (K.A. Khor).

0142-9612/02/$ - see front matter
PII: S0142-9612(02)00413-1

theoretically studied the dissolution dynamics with the use of a kinetic rate law,

$$\frac{dC}{dt} = k_D \left[\frac{K_{SO} - IP}{K_{SO}}\right]^n, \quad (1)$$

where C is the molar quantity being dissolved, t is the incubation time, k_D is a constant, n is the kinetic rate order and $K_{SO} - IP/K_{SO}$ =relative undersaturation. Even though the dissolution behavior is intensely complicated and the coating's dissolution rate was dependent on crystallinity, composition, structure, surface area, and density [8]. Moreover, the dissolution is accompanied simultaneously by reprecipitation, which makes analysis of dissolution mechanism an even more abstruse exercise. However, it is believed that the dissolution process could still be reasonably explained through pertinent diffusion theories.

To date, the precipitation mechanism of thermally sprayed calcium phosphate coating incubated in the SBF is still not judiciously understood. A resonant knowledge on the precipitation behavior could be beneficial for a competent understanding of coating bonding with bone and, hence, useful for the extensive use of the coatings in clinical applications. Furthermore, there is still no available literature focusing on the mechanical property evaluation of the precipitates formed on the calcium phosphate matrix surface following in vitro incubation. Therefore, the present study focused primarily on the investigation into the mechanism of the precipitation process in high velocity oxy-fuel (HVOF) sprayed HA coatings. And the mechanical properties of the precipitates were evaluated in terms of Young's modulus and microhardness through nanoindentation. Structural characterization was also conducted through scanning electron microscopy (SEM), X-ray diffraction (XRD), and Fourier transform infrared spectroscopy (FTIR).

2. Experimental procedures

Calcium phosphate coatings were prepared by the HVOF spraying of fully crystalline HA powders onto primed Ti–6Al–4V substrate [9]. A fully computerized *HV2000* HVOF (Praxair, USA) system with a nozzle diameter of 19 mm was utilized for the coating deposition. Hydrogen was employed as fuel gas with a flow rate of 566 l/min. The flow rate of oxygen was 283 l/min. Powder carrier gas was argon with a flow rate of 19 l/min and the powder feed rate was 6 g/min. The spray distance was set at 250 mm. Phase composition of the as-sprayed calcium phosphate coating is revealed through an XRD analysis, which is shown in Fig. 1(a). Segmented coating samples used for the in vitro test were of the dimension 12 mm × 12 mm in width and length, respectively. And the coating thickness was ~100 μm, while

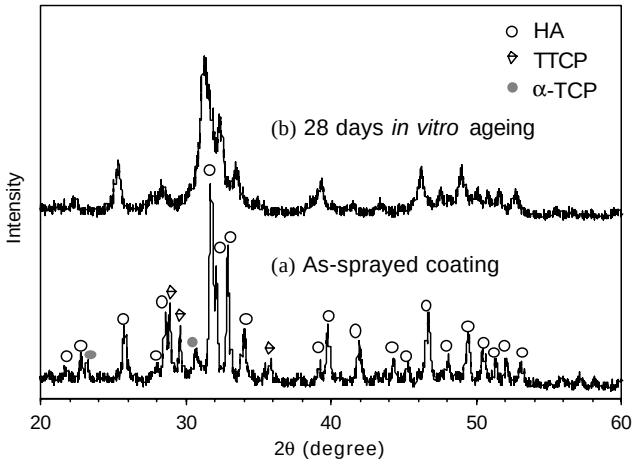

Fig. 1. XRD pattern of the precipitated layer (b) with a comparison to that of starting calcium phosphate coating (a).

Table 1
Composition of the SBF with the comparison to human blood plasma [10]

Ion	Ion concentration (mM) (SBF)	Ion concentration (mM) (blood plasma)
Na^+	142.0	142.0
K^+	5.0	5.0
Mg^{2+}	1.5	1.5
Ca^{2+}	2.5	2.5
Cl^-	147.8	103.0
HCO_3^-	4.2	27.0
HPO_4^{2-}	1.0	1.0
SO_4^{2-}	0.5	0.5

the substrate thickness was 2 mm. The Kokubo SBF (pH = 7.40) [10] was used for the in vitro incubation, and its composition was tabulated in Table 1. The in vitro test was conducted in a continuously stirred bath containing distilled water maintained at 37°C. Each coating sample was incubated in 70 ml of SBF contained in a polyethylene bottle. Once the sample was taken out from the solution, it was washed in distilled water and subsequently dried at ambient temperature. In order to reveal the precipitation mechanism, the changes in thickness of the precipitated layer were investigated. To get an accurate determination of the thickness of the precipitated layer after different incubation duration, the surface of original HA coatings was polished before being immersed into the SBF. For each type of coatings classified according to different immersion duration, a total of three samples were used for an average value and the thickness was measured from the cross-sectional SEM images. In the present study, HA coating samples were also incubated in the SBF with a stable temperature of 39°C besides 37°C aiming to reveal the contribution of thermal diffusion to the overall precipitation. For the tests to reveal the thickness of the precipitated layer, the SBF was refreshed every week.

The coating surface morphology was observed using scanning electron microscopy (SEM, JEOL JSM-5600LV). X-ray diffraction (XRD) analysis (MPD 1880, Philips, The Netherlands) was conducted to reveal phase changes on the coating surface after in vitro ageing in the SBF. The operating conditions were 40 kV and 30 mA by using Cu Kα radiation. The goniometer was set at a scan rate of 0.015° $2\theta/s$ over a 2θ range of 20–60°. Chemistry of the precipitated layer was characterized by Fourier transform infrared spectroscopy (FTIR) analysis (Nicolet Magna FTIR-560). The sample was prepared through scratching an extremely thin layer from the coating surface using a fine-pointed scalpel and the fragments were mixed with dried potassium bromide (KBr) powders at a concentration of around 1 wt% and subsequently compressed to produce a transparent tablet. The infrared spectrum with a resolution of 8 cm^{-1} and the scan number of 4 was adopted with a spectral region from 400 to 4000 cm^{-1}. The concentration of Ca^{2+} in the SBF was measured by using inductively coupled plasma (ICP, Perkin Elmer, Emission Spectrometer Plasma 400) analysis.

Nanoindentation was employed as an effective method for the determination of physical properties of the precipitated layer due to its extremely small test scale [11,12]. The Young's modulus and microhardness of the present samples were determined through nanoindentation on the Nano-Indenter®XP system. The tests were carried out on polished cross-sections of the coating matrix and the precipitated layer. For each test location, a total of 15 data points were amassed for an average value. The load used for the present nanoindentation evaluation was 30 mN.

3. Results and discussion

The changes of phase composition at coating surface after its incubation in the SBF are shown in Fig. 1. Preferential dissolution of the phases α-TCP, TTCP and ACP, which resulted from HA phase transformation during coating formation [9], has been clarified in a previous publication [13]. It is apparent that after 28 days' incubation, only bone-like apatite is detected on the coating surface. Surface and cross-sectional morphologies, which are shown in Figs. 2(a) and (b), respectively, suggest that the precipitated layer is an apatite, which fully covers the coating surface. FTIR analysis result, as shown in Fig. 3, further confirms the phase of the precipitated layer as bone-like apatite. It is noted from the IR curve of the precipitates that the peak labeled at 3570 cm^{-1}, which is assigned to the stretching of hydroxyl (OH^-) group in HA [14] cannot be observed. It alludes to a poorly crystallized structure. The intensities of the well-pronounced absorption bands

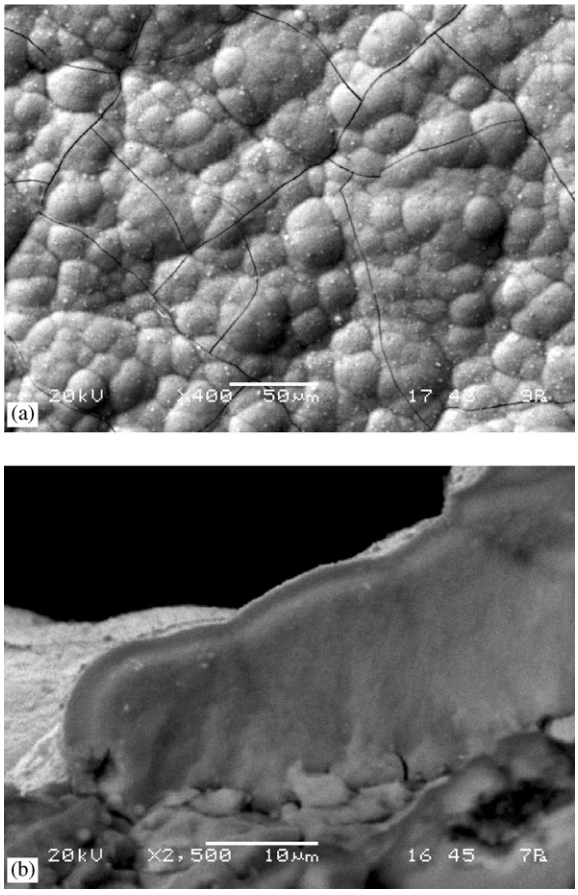

Fig. 2. SEM morphology of the precipitated bone-like apatite from (a) topographical and (b) cross-sectional view.

at 1460, 1419 and 876 cm^{-1}, characteristic of carbonate bands, suggest the precipitated layer as carbonated apatite [15]. And the band labeled at 1644 cm^{-1} represents absorbed water.

As discussed in previous reports [5,6,16], the dissolution was actually a phase-dependent process. Furthermore, from the morphology comparison of coating samples following 24 h of incubation to 6 h of ageing, shown in Fig. 4, it is noted that the precipitation shows a phase-dependent preference. Essentially, the precipitation occurs at specific locations where dissolution took place. It appeared that a fresh surface provided by dissolution is beneficial for molecules attachment. However, it is strongly believed that the phenomenon resulted principally from an intensified local Ca^{2+} concentration. The dissolution of TCP, TTCP or ACP at the coating surface triggered significant increase in Ca^{2+} concentration encompassing the dissolution area, which can effectively accelerate the precipitation process. Meanwhile, it could be claimed that once Ca^{2+} concentration is sufficiently high, attachment of molecules or ions acting as precipitation nuclei is faster than the reverse dilution of the ions via diffusion into the SBF. Therefore, it can be stated that certain dissolution

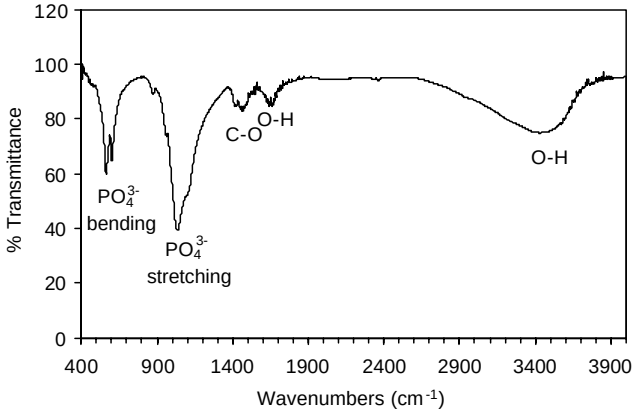

Fig. 3. FTIR curve of the precipitated layer formed on the calcium phosphate coating confirming it is a bone-like apatite.

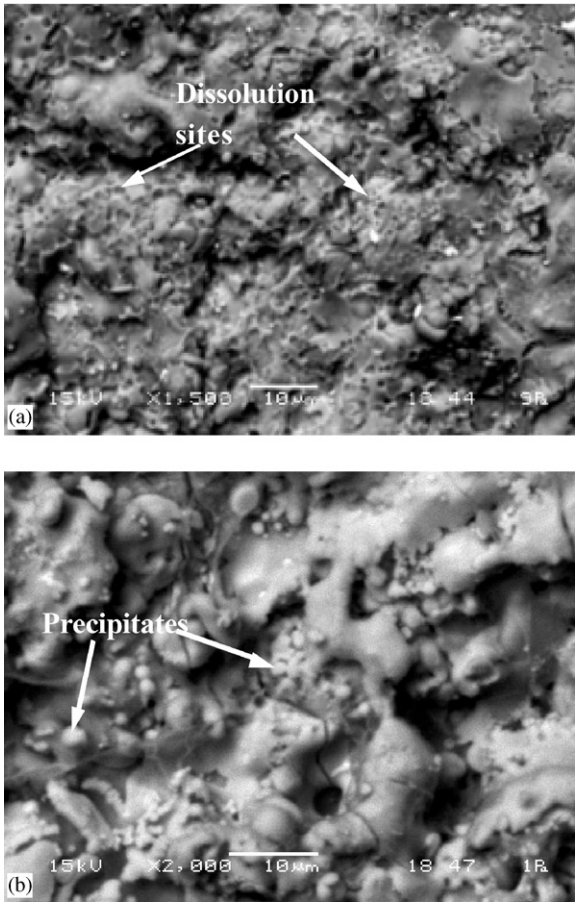

Fig. 4. SEM image of the coating surface in high magnification showing (a) the oriented dissolution with 6 h ageing and (b) the oriented precipitation with the ageing time of 24 h in the SBF.

is beneficial for rapid precipitation. And from this point of view, a uniform distribution of dissolvable phases on the surface of calcium phosphate coatings could be beneficial for expeditious precipitation.

Nanoindentation was conducted on polished cross-sections of the precipitated bone-like apatite layer. Fig. 5 shows Young's modulus and microhardness values of the apatite layer with a comparison to the coating matrix adjacent to the precipitates. Constraints encountered include limited indentation area, from 5.58 to 7.70 μm^2, and minor data standard deviation. Nonetheless, it is found that the apatite formed at the initial stage (<1 week) showed a relatively higher Young's modulus value than that formed during the later stages. From the morphology observation on the cross-sections of the precipitated layer shown in Fig. 6, it is apparent the outer most layer shows different morphology from the original layer in terms of density. This phenomenon could be responsible for the gradual decrease in Young's modulus values, from 123 to 113 GPa, and finally, 110 GPa. The changes in Young's modulus, on the other hand, prove the difference in density of the bone-like apatite layer. Furthermore, the same altering trend exhibited by microhardness, from 4.93 GPa to 4.33 GPa, and finally, 4.21 GPa, confirms the phenomenon suggested by the altered Young's modulus. It should be noted that on the coating side, which is closely adjacent to the apatite layer, the Young's modulus and microhardness show values of 114 and 3.98 GPa, respectively. The Young's modulus within HA coating is 118 GPa together with a microhardness value of 4.21 GPa. It is noted that the tests were carried out at locations with dense structure. Regarding the extremely limited indentation area, the high E values could correspond to certain specific phases. As discussed earlier, precipitation was a crystal-oriented process and was directly related to dissolution and TCP and ACP showed higher dissolvability than crystalline HA [5,17]. The small decrease of Young's modulus exhibited by point B compared to point A within the HA coating may confirm that assumption. Furthermore, through the nanoindentation test with the same operation parameters, cross-sections of the starting HA powders exhibits an average Young's modulus value of 83.9 GPa (± 9.4 GPa) and a microhardness value of 5.22 GPa (± 0.87 GPa). It is noted that compared to the nanoindentation result on bulk HA coating, which was exhibited in Fig. 5, the starting HA particles showed relatively low Young's modulus values. Since the starting powders have essentially stress-free structures, it can therefore be asserted that the residual stresses formed during HVOF coating formation could be responsible for the enhanced E values exhibited by the HA coatings, as measured by nanoindentation. From this point of view, the release of residual stresses at coating surface during in vitro incubation is partially responsible for the decreased Young's modulus.

In order to ascertain the precipitation mechanism further, the alterations in thickness of the precipitated layer were investigated. It was revealed that for the calcium phosphate coatings without surface treatment, the precipitated layer showed a modified thickness.

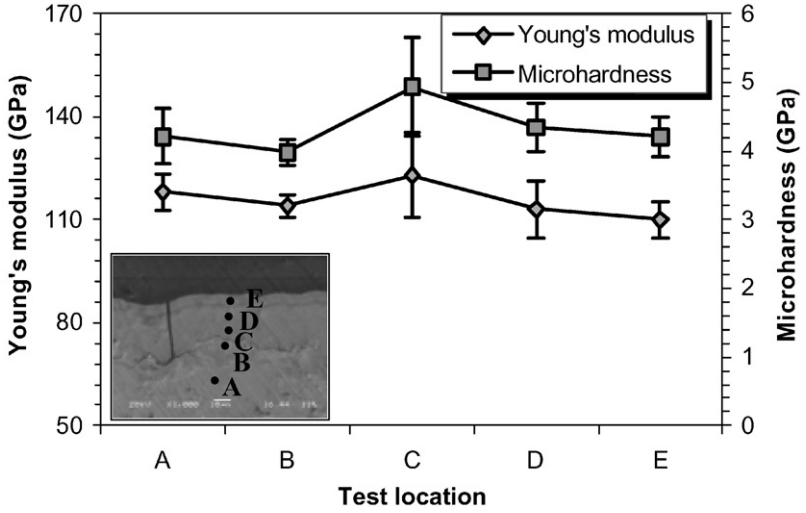

Fig. 5. *E* and microhardness values of the precipitated layer with the comparison to the HA coatings closely adjacent to the precipitates obtain from the nanoindentation test.

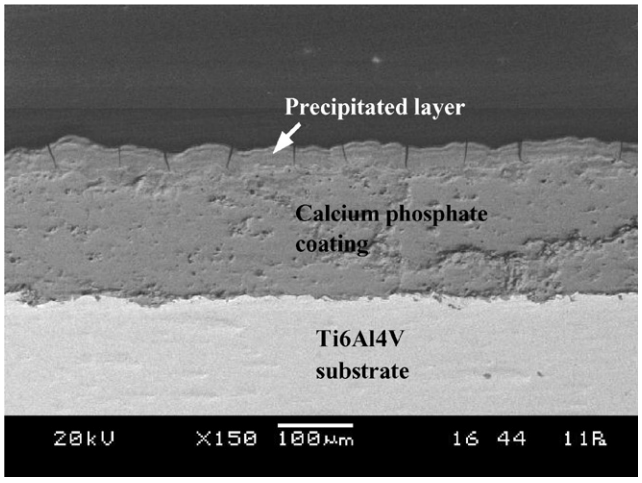

Fig. 6. Typical cross-sectional morphology of the precipitated layer on the polished HA coating surface showing a unique thickness.

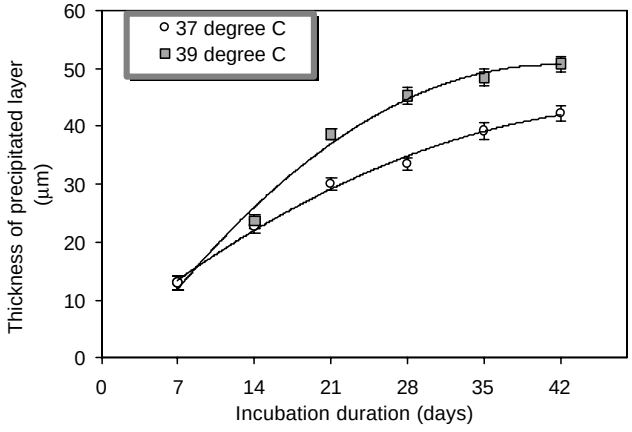

Fig. 7. Changes in thickness of the precipitated layer versus the incubation duration in vitro claiming a partially diffusion-controlled precipitation.

Therefore, in order to get the actual thickness of the precipitated layer after different incubation duration, the surface of the original HA coatings were polished using 1-μm diamond paste before being immersed into the SBF. Fig. 6 shows a typical morphology that a unique thickness of the apatite layer is manifested on the polished coating surface. Fig. 7 shows the influence of incubation duration on the thickness of the precipitated layer. It should be noted that, for the purpose of revealing the influence of solution temperature on the precipitation process, all the samples were incubated in the 37°C SBF in the first week on the basis that, for the present coating, 7 days of incubation has brought about identified precipitation [13]. From Fig. 7, it is noted that the thickness of the precipitated layer augments with the incubation time and higher solution temperature results in accelerated precipitation. For both tests, a regressive curve relating the thickness of the apatite layer to incubation duration was obtained. Since the SBF was refreshed once a week, the difference in the layer thickness indicates the important contribution of diffusion of the ions, Ca^{2+}, PO_4^{3-}, and others, in the SBF to the precipitation. However, it was noted that the difference in thickness was 0.8, 8.6, 11.8, 9.3 and 8.5 μm corresponding to the immersion duration of 14, 21, 28, 35 and 42 days, respectively. This suggests that, besides diffusion, other processes could also be accountable for the overall precipitation, which could include the further dissolution around the through-thickness cracks as demonstrated in Fig. 2(a). In order to reveal the dissolution behavior, the coating samples were also incubated in the SBF without being periodically

refreshed. The concentration changes of Ca^{2+} in the SBF further confirm the contribution of diffusion to the overall precipitation, which is shown in Fig. 8. It is noted that, as the SBF was not refreshed, precipitation could be extremely limited as the Ca^{2+} concentration in the SBF is low. The large concentration difference brought about mainly by dissolution is the reason for the high rate of precipitation during the early stage of incubation. Furthermore, the altered thickness of the precipitates also indicates the contribution of dissolved ions from the coating matrix to the overall precipitation, which has been proven by previous studies [17]. It can therefore be concluded that the precipitation of the bone-like apatite is a partial diffusion-controlled process.

As mentioned previously, it was found that the precipitation originally occurred at the place where dissolution took place. And the precipitation was found to be a partially diffusion-controlled process. As a matter of fact, the bulk bone-like apatite layer formation should originally come from initial attachment of a single molecule. Kinetic and other local effects may also produce transient changes in shape, despite the fact that a sphere presents the lowest area, and thus the lowest energy state, of the phase interface. For simplicity, a molecule could be considered to be spherical as it approaches a solid surface as a liquid. Provided it will stick or adhere to the surface, the work of adhesion is generally described as (for adhesion of phase A–B) [3]

$$W_{AB} = \gamma_A + \gamma_B - \gamma_{AB}, \tag{2}$$

where γ_A and γ_B are free surface tensions, γ_{AB} is the interfacial surface tension. For this situation, it can be written as

$$W_{SP} = \gamma_{SL} + \gamma_P - \gamma_{PS}. \tag{3}$$

W_{SP} must be negative for adhesion to take place (S represents solid, L represents liquid, P is the molecule). Kinetic rate law has been employed for the explanation of dissolution behavior in the SBF [5]. The precipitation process can be schematically described as shown in Fig. 9. The precipitation mechanism involves the determination of free surface tensions of TCP and HA, as well as the bone-like apatite. It has been pointed out that apatite is the most thermodynamically favored phase to precipitate [4]. The precipitated apatite showed relevant crystal structure to the calcium phosphate matrix and the implantation site also demonstrated remarkable influence on the apatite precipitation [18]. Moreover, an in vivo test showed that both HA crystals and precipitated microcrystals had the same *d* spacing and the same apatite structure [18]. In the present study, the oriented precipitation supports the evidence of the determinant effect of different phases on the determination of molecule attaching sites. However, it is still not clear on the locations on the calcium phosphate matrix where the precipitation occurred.

Since the components of the SBF solution is multi-chemicals, while the final phase precipitated on HA coating surface is a bone-like apatite, the exact formation of this phase is still not well understood, considering that the dynamics of the process at the molecular level has not been well established. Nevertheless, a previous study has shown that the precipitation rate of the bone-like apatite on their surface was in the order: β/α-TCP (β-TCP contains some α-TCP) > HA > Ti > ACP [4]. And poorly crystallized coatings that resorbed faster showed greater surface film precipitation and greater chemical changes than amorphous coatings [17]. It suggests that the crystalline structure is indeed important in dictating the differences in the rate of nucleation.

Since it was claimed that the precipitation was a partial diffusion-controlled process, the interaction potentials between single molecules or ions and matrix

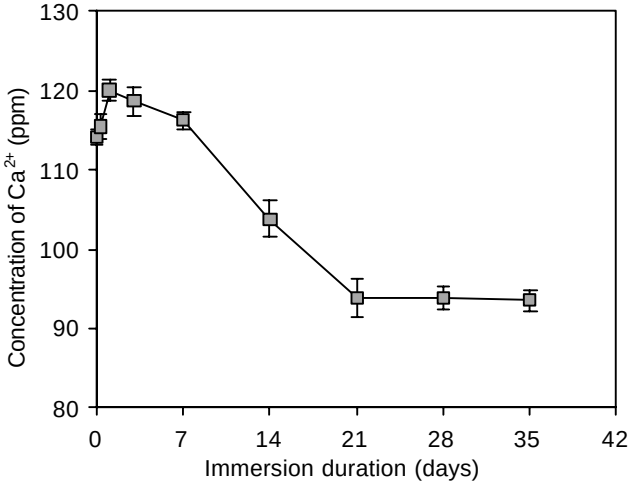

Fig. 8. Ca^{2+} concentration in the SBF via immersion duration of the HA coating samples (the SBF was not refreshed during the experiments).

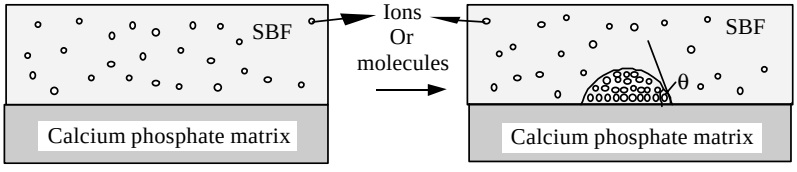

Fig. 9. Depiction of the precipitation of bone-like apatite on the calcium phosphate matrix.

surface should be clarified. The net interaction energy, w, for a molecule at a distance, D, away from the surface can be determined according to the following formula [19]:

$$w(D) = -2\pi C\rho/(n-2)(n-3)D^{n-3} \quad \text{for } n > 3, \tag{4}$$

where w is the net interaction energy, D is the distance of the molecule or ion away from the matrix surface, ρ is the number density of molecules in the matrix solid (as discussed earlier, the precipitated matrix is an accumulation of molecules), and C is the interaction constant. If only van der Waals forces are considered, then $n = 6$ [19]

$$w(D) = -\pi C\rho/6D^3. \tag{5}$$

The corresponding force can be determined as $F = \partial w(D)/\partial D = -\pi C\rho/2D^4$. It is hence revealed that the precipitation rate is directly related to the density of the pre-precipitated layer. This could be the partial reason why at the incipient stage of incubation that once the coating surface was fully covered by the precipitated apatite, the accumulation rate was noticeably fast. It is obvious that the surface dissolution is one of the steps leading to quick calcium phosphate precipitation and subsequent tissue bonding. The precipitation rate was found to depend principally on the dissolution rate. And once the coating surface is completely covered by the attached spheres, further dissolution is distinctly minimized.

4. Conclusion

Bone-like apatite layer that precipitated on HVOF sprayed calcium phosphate coating surface following in vitro evaluation was characterized. It was found that the dissolution of TCP, TTCP, or ACP phases at the coating surface accelerated the precipitation of the dense apatite achieved through significant increase of Ca^{2+} concentration at a localized area. The investigation confirmed that the precipitation rate was directly dependent on the Ca^{2+} concentration in the SBF at the vicinity of the coating surface. The Young's modulus of the precipitated apatite layer showed a value of $\sim$120 GPa obtained from nanoindentation. The analysis of the apatite deposition mechanism lent weight to the perception that the precipitation of bone-like apatite on the HA coating was most likely a partially diffusion-controlled process.

References

[1] Hardy DCR, Frayssinet P, Delince PE. Osteointegration of hydroxyapatite-coated stems of femoral prostheses. Eur J Orthop Surg Traumatol 1999;9:75–81.

[2] Yoshikawa T, Ohgushi H, Tamai S. Immediate bone forming capability of prefabricated osteogenic hydroxyapatite. J Biomed Mater Res 1996;32:481–92.

[3] Black J. Biological performance of materials, fundamentals of biocompatibility, 3rd ed. (revised and expanded). New York: Marcel Dekker, USA, 1999.

[4] Cleries L, Fernandez-Pradas JM, Morenza JL. Behavior in simulated body fluid of calcium phosphate coatings obtained by laser ablation. Biomaterials 2000;21:1861–5.

[5] Ducheyne P, Radin S, King L. The effect of calcium phosphate ceramic composition and structure on in vitro behavior, I. Dissolution. J Biomed Mater Res 1993;27:25–34.

[6] Harada Y, Wang JT, Doppalapudi VA, Willis AA, Jasty M, Harris WH, Nagase M, Goldring SR. Differential effects of different forms of hydroxyapatite and hydroxyapatite/tricalcium phosphate particulates on human monocyte/macrophages in vitro. J Biomed Mater Res 1996;31:19–26.

[7] Reis RL, Monteriro FJ. Crystallinity and structural changes in HA plasma-sprayed induced by cyclic loading in physiological media. J Mater Sci Mater Med 1996;7:407–11.

[8] Wise DL, Trantolo DJ, Lewandrowski K-U, Gresser JD, Cattaneo MV, Yaszemski, MJ, editors. Biomaterials engineering and devices: human applications, vol. 2: orthopedic, dental, and bone graft applications, Totowa, NJ: Humana Press, 2000.

[9] Li H, Khor KA, Cheang P. Effect of the powders' melting state on the properties of HVOF sprayed hydroxyapatite coatings. Mater Sci Eng A 2000;293:71–80.

[10] Kokubo T, Kushitani H, Sakka S, Kitsugi T, Yamamuro T. Solutions able to reproduce in vivo surface changes in bioactive glass-ceramic A-W[3]. J Biomed Mater Res 1990;24:721–4.

[11] Oliver WC, Pharr GM. An improved technique for determining hardness and elastic modulus using load and displacement sensing indentation experiments. J Mater Res 1992;7:1564–83.

[12] Woirgard J, Dargenton JC, Tromas C, Audurier V. A new technology for nanohardness measurements: principle and applications. Surf Coat Technol 1998;100–101:103–9.

[13] Li H, Khor KA, Cheang P, Boey SY. In vitro behavior of HVOF sprayed calcium phosphate splats and coatings. Biomaterials, in press.

[14] Wang BC, Chang E, Yang CY, Tu D, Tsai H. Characteristics and ostoconductivity of three different plasma-sprayed hydroxyapatite coatings. Surf Coat Technol 1993;58:107–17.

[15] Radin SR, Ducheyne P. The effect of calcium phosphate ceramic composition and structure on in vitro behavior: II. Precipitation. J Biomed Mater Res 1993;27:35–45.

[16] Gross KA, Berndt CC. In vitro testing of plasma-sprayed hydroxyapatite coatings. J Mater Sci Mater Med 1994;5:219–24.

[17] Maxian SH, Zawadsky JP, Dunn MG. In vitro evaluation of amorphous calcium phosphate and poorly crystallized hydroxyapatite coatings on titanium implants. J Biomed Mater Res 1993;27:111–7.

[18] Rohanizadeh R, Trecant-Viana M, Daculsi G. Ultrastructural study of apatite precipitation in implanted calcium phosphate ceramic: influence of the implantation site. Calcif Tissue Int 1999;64:430–6.

[19] Israelachvili JN. Intermolecular and surface forces, 2nd ed. New York: Academic Press, Harcourt Brace & Company, 1992.